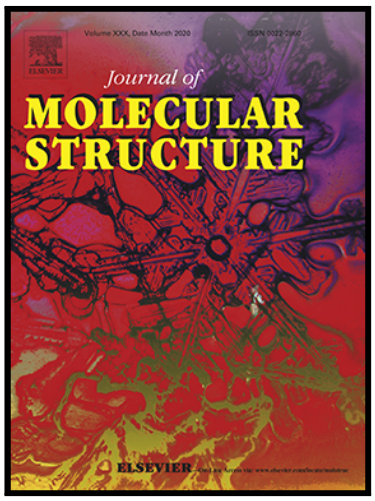

Structural, spectroscopic and biological study of trifluoroethyl methansulfonate (methylsulfonyl), TFMSMS

J.E. Galván , Contreras Aguilar , S.E. Ulic , R.D.I. Molina , M.E. Arena , S.B. Diaz , A. Ben Altabef , M.E. Tuttolomondo

PII: S0022-2860(22)00664-0
DOI: https://doi.org/10.1016/j.molstruc.2022.133000
Reference: MOLSTR 133000

To appear in: *Journal of Molecular Structure*

Received date: 14 September 2021
Revised date: 25 February 2022
Accepted date: 3 April 2022

Please cite this article as: J.E. Galván , Contreras Aguilar , S.E. Ulic , R.D.I. Molina , M.E. Arena , S.B. Diaz , A. Ben Altabef , M.E. Tuttolomondo , Structural, spectroscopic and biological study of trifluoroethyl methansulfonate (methylsulfonyl), TFMSMS, *Journal of Molecular Structure* (2022), doi: https://doi.org/10.1016/j.molstruc.2022.133000

Highlights

- The experimental and theoretical study on the molecular and vibrational analysis of Trifluoroethyl methansulfonate (methylsulfonyl), TFMSMS is presented.
- The IR and Raman spectra were recorded in solid state and compared with the spectral data obtained by the DFT/B3LYP method using the 6-311G(3df) basis set.
- This is the first study on the Trifluoroethyl methansulfonate (methylsulfonyl), TFMSMS, on biofilm formation and the first study on a TFMSMS with respect to QS activity.

Structural, spectroscopic and biological study of trifluoroethyl methansulfonate (methylsulfonyl), TFMSMS

J. E. Galván[1], Contreras Aguilar[2], S. E. Ulic[2,3,*] sonia@quimica.unlp.edu.ar, R. D. I. Molina[4], M.E. Arena[4], S. B. Diaz[1], A. Ben Altabef[1], M. E. Tuttolomondo[1,*] metdemunoz@yahoo.com

[1]INQUINOA-CONICET, Instituto de Química Física, Facultad de Bioquímica, Química y Farmacia, Universidad Nacional de Tucumán, R. Argentina

[2]CEQUINOR (CONICET-UNLP), Facultad de Ciencias Exactas, Universidad Nacional de La Plata, 120 N° 1465 (1900) La Plata, R. Argentina

[3]Departamento de Ciencias Básicas, Universidad Nacional de Lujan, Ruta 5 y 7, 6700 Luján, Buenos Aires, R. Argentina

[4]INBIOFAL-CONICET (Instituto de Biotecnología Farmacéutica y Alimentaria) Universidad Nacional de Tucumán, R. Argentina

*Corresponding authors

Abstract

Trifluoroethyl methansulfonate (methylsulfonyl), **TFMSMS** is a new compound derived from Clomesone, which was obtained in solid state. As no experimental geometric parameters were available, a conformational exploration was carried out (using the concept of "conformational transferability"), resulting a single stable conformation at room temperature. Infrared, Raman, and liquid NMR spectra were measured. The contributions of the donor → acceptor interaction energies were also analyzed by Natural Bond Orbitals (NBO) approximations and topological properties (AIM). These results evidenced that electron delocalization and especially LP O→σ*O(3)-C(3) interaction play an important role in the reactivity-structure

connection of oxoesters and thioesters. TFMSMS could partially inhibit growth and biofilm formation on Pseudomonas aeruginosa and Staphylococcus aureus strains. Moreover, this is the first study demonstrating the methansulfonate complex interference with the Quorum sensing system in Gram-negative bacteria.

Graphical Abstract

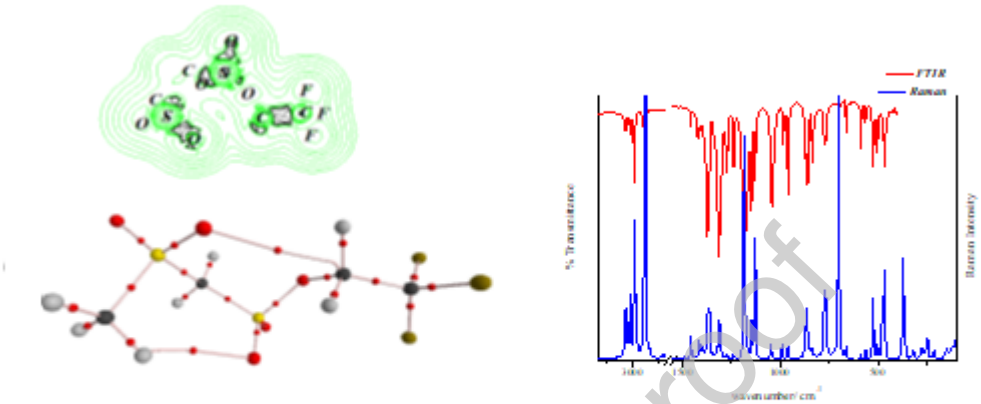

Keywords

FTIR and Raman spectroscopies / NBO calculations / *ab initio* calculations.

1. INTRODUCTION

Trifluoroethyl metansulphonate (methylsulfonyl), **TFMSMS**, synthesized for the first time in this work is a new compound derived from Clomesone. This type of compound is of biological interest. They are alkylating agents which can react with nucleophilic centers of biological macromolecules, specifically DNA molecules, binding either to heterocycles or to phosphate groups. Due to these characteristics, they are considered antineoplastic substances that prevent the development or growth of malignant tumor cells. [1-5]

When fluorinated substituents are used, they can cause opposite electronic effects. The high electronegativity of the F atom generates a strong inductive effect (-I), thus attracting the electron density of the structure. However, the donation of electron density can also be carried out by a mesomeric effect (+ M).[6] Furthermore, the presence of F as a substituent improves the properties of the compounds related to their activity and toxicity. Pharmacological studies on compounds that have trifluoromethyl

groups (CF_3) show several medicinal properties. [6] Numerous studies reveal the influence of fluorine atoms on the lipophilicity of the molecule, which modifies the distribution of drugs in the membrane, causing a decrease in the observed toxicity. [7-9] The synthesis of a fluorinated derivative of Clomesone, [10] replacing the CH_2Cl by a CF_3 group considered as one of the most lipophilic substituents, could have more far-reaching effects.

The aim of this work is to provide information about the structure and spectroscopic properties (NMR, FTIR and Raman) of **TFMSMS**, with the assistance of theoretical calculations. The stability of the compound in terms of hyper-conjugative and charge transfer interactions has been studied through the Second Order Perturbation Theory of the Fock Matrix by means of the NBO analysis. [11] The AIM theory, [12] has been used to analyze the topology of all optimized structures.

The mistaken and excessive use of antibiotics and disinfectants causes the development of bacteria resistant to clinical and disinfection treatments. It is known that the formation of biofilm, a biological film that prevents the contact of bacteria and to medium metabolites, decreases the effectiveness of antimicrobial agents. The biofilm is the predominant form in which bacteria are found in the environment and is controlled by a chemical system of bacterial communication, called Quorum sensing (QS). For these reasons, inhibiting the QS and biofilm is a new target in the study of antimicrobial compounds. [13] Several studies were carried out in both species with natural [14] and synthetic products [15] to find new bioactive compounds. [16,17]

This new fluorinated methansulfonate derivative was also evaluated as an inhibitor of bacterial growth, biofilm formation of *Pseudomonas aeruginosa* and *Staphylococcus aureus* as well as the inhibition ability of QS Gram-negative signaling, using the biosensor strain Chromobacterium violaceum CV026.

2. EXPERIMENTAL

2.1. Synthesis of trifluoroethyl metansulphonate (methylsulfonyl)

Trifluoroethyl methansulfonate (methylsulfonyl), TFMSMS, was prepared as reported in the literature [18] with slight modifications. In a round-bottom flask, 3mL of methanesulfonyl chloride dissolved in 3mL acetonitrile was added drop-wise under stirring to a solution of triethylamine (8 mL) in acetonitrile (17.5 mL). The mixture was kept at -30°C for 1 hour. Then, a solution of 2-trifluoroetanol (1.3 mL) in 1.3 mL of acetonotrile was added and stirred for two hours.

The white solid (Et_3NHCl) was filtered at room temperature, the solution was washed with NaCl 0.1M, dried over Na_2SO_4 and evaporated *in a vacuum* to give an orange-red oil. The crude product was dissolved in a mixture of dichloromethane: hexane and stored overnight at -5ºC. The solid ($CH_3SO_2CH_2SO_2$-O-CH_2CF_3) was filtered, washed with cold hexane and recrystallized twice from hot chloroform. The obtained white crystalline solid was suitable for spectroscopic and structural studies. The crystals were too small for X-ray diffraction.

2.2. NMR spectroscopy

The observed shifts are consistent with the expected ones, especially those of the deshielded nuclei (CH_3 and CH_2) due to the presence of the sulfone ($S(17)O_2$) and sulfonate ($S(18)O_3$) groups, respectively. In addition, the C-F and H-F heteronuclear couplings allowed to identify the ^{13}C and ^{1}H atoms linked to two and three bonds, respectively, as quartet signals. The spin system formed by the -CH_2-SO-CH_3 group as two signals with quartet (q, CH_2) and triplet (t, CH_3) multiplicity, was assigned considering the homonuclear H-H coupling while the respective ^{13}C signals are singlets.

^{1}H NMR (400 MHz, $CDCl_3$) δ = 4.72 (q, $^{3}J_{HF}$ = 7.8 Hz, 2H, **C<u>H</u>$_2$**-CF_3), 4.70 (q, $^{4}J_{HH}$ = 0.8 Hz, 2H, **C<u>H</u>$_2$**), 3.26 (t, $^{4}J_{HH}$= 0.8 Hz, 3H, **C<u>H</u>$_3$**).

^{13}C NMR (101 MHz, $CDCl_3$) δ = 121.68 (q, $^{1}J_{CF}$ = 278 Hz, **<u>C</u>F$_3$**), 69.32(s, **<u>C</u>H$_2$**), 67.60 (q, $^{2}J_{CF}$ = 39 Hz **<u>C</u>H$_2$**-CF_3), 42.44 (s, **<u>C</u>H$_3$**).

2.3. Vibrational spectroscopy

The FTIR spectra were recorded in the range of 4000-400 cm^{-1}, with a spectral resolution of 2 cm^{-1}, using a Perkin-Elmer GX1 FTIR spectrometer. The Raman spectrum of the solid was measured in the 3500–100 cm^{-1} region with a Thermo Scientific DXR Raman microscope, and a resolution of 5 cm^{-1}. The Raman data were collected using a diode-pump solid state laser of 532 nm. The ^{1}H and ^{13}C NMR spectra of **TFMSMS** were recorded on a Bruker Avance 300 and Bruker Avance 250, respectively, using $CDCl_3$ as solvent and TMS as internal standard.

2.4. Computational details

The Gaussian 03-09[19-20] set of programs was used to carry out DFT calculations. Full optimizations were performed with standard gradient techniques at the DFT levels of theory. Pople´s 6-31G(d), 6-311(3df) and 6-311++G**[21-24] basis sets were used.

Becke-3-parametrLee-Yang-Parr (B3LYP) hybrid functional [25-29]was employed for correlation. In addition, Natural Bond Orbital (NBO) calculations were performed at the B3LYP/6-311G(3df) level of theory using the NBO 3.1 program. [30,31] AIM calculations were carried out using the AIM2000 program. [32] The atomic displacements given by the Gaussian program for each vibrational mode were used to understand qualitatively the nature of the molecular vibrations and, for that purpose; the corresponding data were represented graphically using the GaussView program. [33] The calculated frequencies were scaled using the Yoshida methodology, [34] and the potential energy distribution (PED) was calculated by means of the VEDA program. [35]

The population was calculated according to a Boltzmann distribution:

$$\%pop_i = \frac{e^{-\Delta G_i/RT}}{\sum_{k=1}^{n} e^{-\Delta G_k/RT}} \times 100\% \quad (1)$$

2.5. Bacterial growth

Overnight cultures of *Pseudomonas aeruginosa* PAO1, *Pseudomonas aeruginosa* PA14 and *Staphylococcus aureus* ATCC 6528 were diluted to reach an optical density (OD) of 0.125 ± 0.01 at 560 nm in Luria-Bertani (LB) and Müeller Hinton (MH) medium, respectively. The diluted culture (195 µL) was placed in one of the 96 wells of a microtitre polystyrene plate. Solutions of **TFMSMS** in dimethyl sulphoxide (DMSO, Sigma–Aldrich) were prepared separately, and 5 µl of each one was pipetted to the microtitre plate wells individually (5 replicates) to reach final concentrations of 200, 100, and 10 µg/mL.

Control wells (5 replicates) contained the diluted culture (195 µL) and 5 µL of DMSO, in which the final concentration of DMSO was 2.5%. Bacterial cultures were grown at 37°C for 24 h and growth was detected as turbidity (560 nm) using a microtitre plate reader (Thermo Fisher Multiscan Go, Finland). Ciprofloxacin was incorporated in the same bioassay as a positive control at 1 µg/mL.

2.6. Biofilm formation assay

For biofilm quantification, a micro method based on a protocol previously reported was employed. [36] The supernatants of bacterial cultures prepared as described earlier was discarded after 24 h incubation, and the material that remained fixed to the polystyrene

(containing biofilm) was washed with water. Biofilms formed were stained with 200 µL of an aqueous solution of crystal violet (0.1% w/v) for 30 min. After washing with water, crystal violet bound to biofilm was removed from each, employing 200 µl of absolute ethanol and shaking for 30 min at 37°C. Absorbance (580 nm) crystal violet in ethanol solutions was determined using the microtitre plate reader.

2.7. Biosensor assay

Detection of QS inhibition was performed by a diffusion assay using the biosensor strain *Chromobacterium violaceum* CV026. The strain is a Tn5- mutant unable to produce the pigment violacein *per se*, due to lack of autoinducer production. However, Tn5- mutant can form violacein and depends on the exogenous addition of autoinducers. [37] Wells were made in the center of the LB agar plates surfaces, previously inoculated with *C. violaceum* CV026 and supplemented with 5 µg of the autoinducer N-hexanoyl-L-homoserine lactone (HHL) (Sigma). The wells were loaded with 50 µl of a 4 mg/ml solution of **TFMSMS** dissolved in DMSO to obtain 200 µg per well. DMSO was included as a solvent vehicle control. After incubating for 18 h at 28 °C, QS inhibition was visualized.

If the compounds affect bacterial growth, no turbidity or pigmentation will be observed near them, with a clear halo without the presence of viable cells (turbidity) or production of violacein around the well.

However, cloudy halos on a purple background indicate inhibition of QS without affecting microbial growth. The anti-QS effect is due to the antagonist molecules that bind instead of the natural auto inductive ligands and prevent the DNA from binding to the pigment transcript. This effect is epidemiologically significant since violacein is considered an important virulence factor of *C. violaceum*. [38]

2.8. Statistical data analysis

All experiments were conducted in quintuplicates at least three times. Differences in the mean values were evaluated by analysis of variance (ANOVA). The Tukey test was used for all pair-wise multiple comparisons of groups. In all analyses, values of $p < 0.05$ were considered statistically different. [39,40]

3. RESULTS AND DISCUSSION

3.1. Structural calculations

Although **TFMSMS** is a crystalline solid, its molecular structure could not be elucidated by X-ray diffraction. The concept of "transferability" of conformational behavior, that is, the properties by which similar groups adopt the same conformation when they are present in different molecules,[10,47-50] was used to determine its structure. The conformational search was performed by scanning the potential energy curves as a function of the COCS; CCOS; OSCS and SCSC dihedral angles variation. The most stable conformer was determined from the potential energy minima obtained for each dihedral angle of the molecule. The potential energy curves were calculated with the DFT method and using the B3LYP functional with the following bases: 6-31g (d), 6-311g (d, p) and 6-311 ++ g (d, p). [10,41-45] The curves are shown in **Figure 1.**

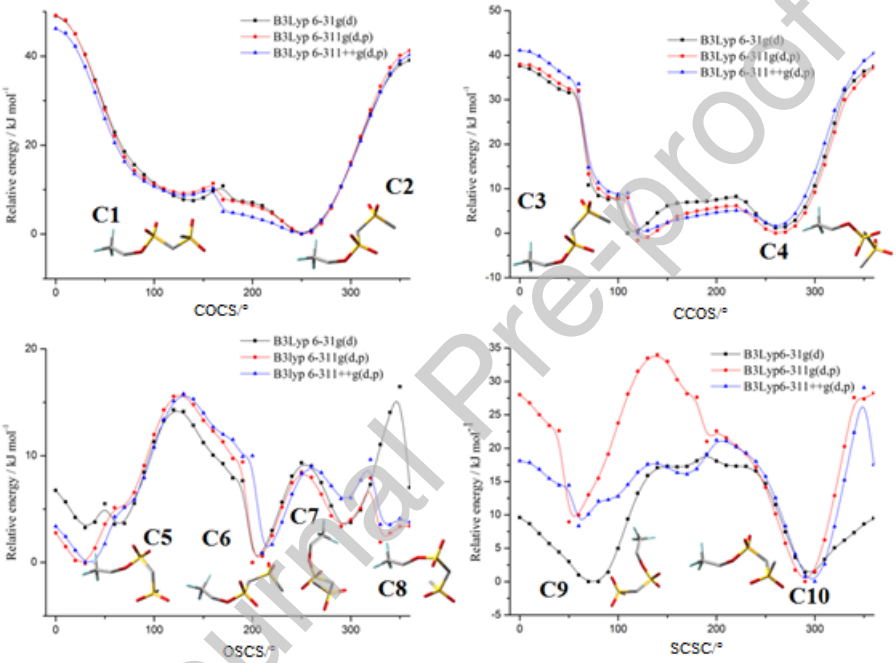

Figure 1. Potential energy curves calculated for the COCS; CCOS; OSCS and SCSC dihedral angles at different levels of theory.

The curves predict the existence of ten different conformations, three of which are the most stable with differences in free energy (ΔG) of about 8 kJ mol^{-1} **(Table S1)**. Based on the free energies values, obtained with B3LYP/6-311++g(d,p) method, the populations were calculated using the Boltzman equation. Only three calculated populations were relevant: 94.7 % for the *C10* conformer shown in **Figure 2** (*quasi-gauche, gauche, gauche, gauche)*; 2.8% for the *C5* conformer (*gauche, gauche, quasi syn, quasi syn)* and 2.4% for the *C2* conformer (*gauche, (-) gauche, (-) anti, gauche).* Considering the populations' values obtained for *C5* and *C*2, the study will be focused

on the *C10* conformer. The *gauche* results in the preferred conformation, particularly by sulfonates and sulfones. [10,41-45]

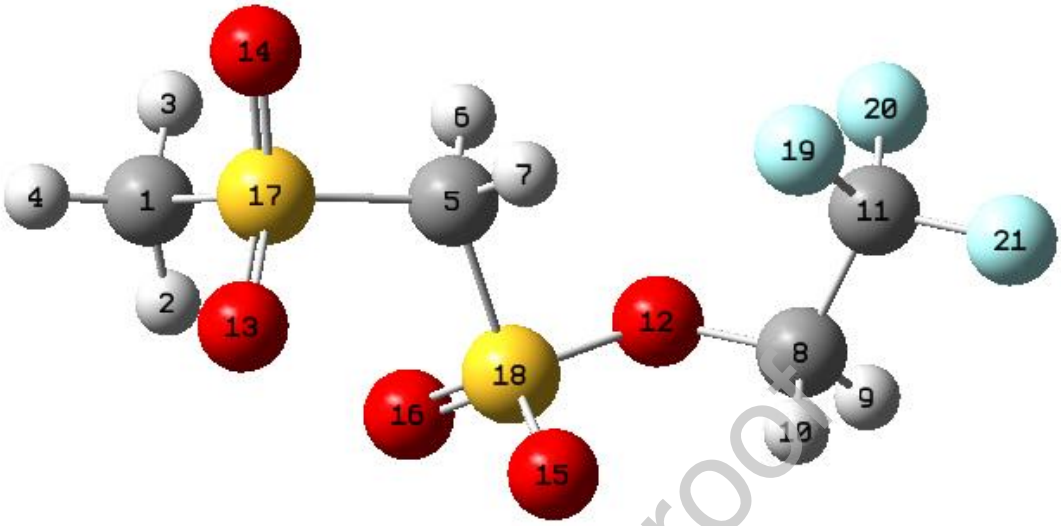

Figure 2. Calculated structure for *C10* conformer (*cg, g, g, g*), including the atoms numbering for **TFMSMS**.

The **TFMSMS** crystal structure could not be resolved by X-ray diffraction, but its geometry was optimized using DFT methods with the functional B3LYP and the 6-311G (d, p), 6-311G (3df) and 6-311 ++ G (3df) bases.

Using the concept of conformational transferability, the structural parameters calculated for **TFMSMS** were compared (**Table 1**) with those obtained by X-ray diffraction for Clomesone, [10] since both molecules have the same functional groups but replace CH_2-Cl by CF_3. As found for the related compounds, [10,41-45] the inclusion of extra polarization functions (beyond a single d function) is necessary to predict accurately the bond lengths in this type of molecules.

A basis set size test, using the B3LYP functional, shows differences in bond distances of less than 5.8 pm. The most sensitive parameter to this orbital description is the X–S bond, which results shortened by 5 pm when replacing the 6-311G (d) basis set by 6-311G (3df). All bonds involving the sulfur atom were shortened around 1 pm, while other bond lengths remain unchanged.

As observed in **Table 1**, the bond distances are similar in both compounds, except for the distance O(12) -C(8), which is shorter for the fluorinated compound. This fact could be attributed to a greater inductive effect of the CF_3 group.

A reliable comparison of the dihedral angles between **TFMSMS** and Clomesone cannot be made, since the crystalline structure of the latter revealed the existence of very strong hydrogen bonds in addition to the Cl-Cl interactions, which affect the value of these angles. Moreover, the TFMSMS structure is stabilized by weak intramolecular hydrogen bonds, resulting in C(1)-H(2)...O(16) and C(5)-H(7)...O(15) the strongest ones. The first interaction is like that found in Clomesone, with an identical hydrogen bond distance (**Table 1**).

Table 1. TFMSMS calculated bond distances at different levels of theory and experimental and calculated values for Clomesone.

Distances(Å)	Rx[a]	B3LYP			
		6-311g(3df)[a]	6-311++g(d,p)	6-311g(3df)	6-311++g(3df)
C(1) $H_{average}$	0.96	1.089	1.089	1.089	1.089
C(1) S(17)	1.747	1.782	1.839	1.781	1.781
S(17) O(13)	1.418	1.435	1.462	1.435	1.438
S(17) O(14)	1.429	1.439	1.465	1.438	1.441
S(17) C(5)	1.801	1.823	1.839	1.825	1.817
C(5) H(6.7)	0.97	1.090	1.090	1.089	1.089
C(5) S(18)	1.776	1.797	1.816	1.796	1.798
S(18) O(15)	1.41	1.427	1.444	1.426	1.424
S(18) O(16)	1.416	1.427	1.456	1.427	1.433
S(18) O(12)	1.566	1.602	1.632	1.617	1.593
O(12) C(8)	1.471	1.445	1.438	1.428	1.434
C(8) $H_{average}$	0.97	1.091	1.090	1.090	1.090
C(8) C(11)	1.476	1.507	1.520	1.520	1.521
C(11) $F_{average}$	-		1.345	1.340	1.340
C(1)-H(2)···O(16)	2.60	2.47	2.44	2.44	2.44

[a](Ref. 10)

3.2. Vibrational analysis

TFMSMS exhibits C_1 symmetry and therefore its 57 normal modes of vibration are IR and Raman active. The vibrational spectra are presented in **Figure 3** and the observed and calculated frequencies in **Table S2**.

The experimental IR and Raman spectra of **TFMSMS** were compared with those calculated (B3LYP/6-311++G(3df)) for the optimized structures of the *C2*, *C5* and *C10* (94%) conformers, in the region of 3200 - 2800 cm^{-1} (**Figure S1**). The observed and calculated IR and Raman frequencies together with PED mode assignments are compiled and the natural internal coordinates in **Tables S2-S3** respectively.

The assignment of the fundamental vibrational modes was carried out by comparison of the frequencies and band intensities of the most abundant conformer (*C10*) with those of related molecules [10,41-45] and with the theoretical graphic representation of the atomic displacements.

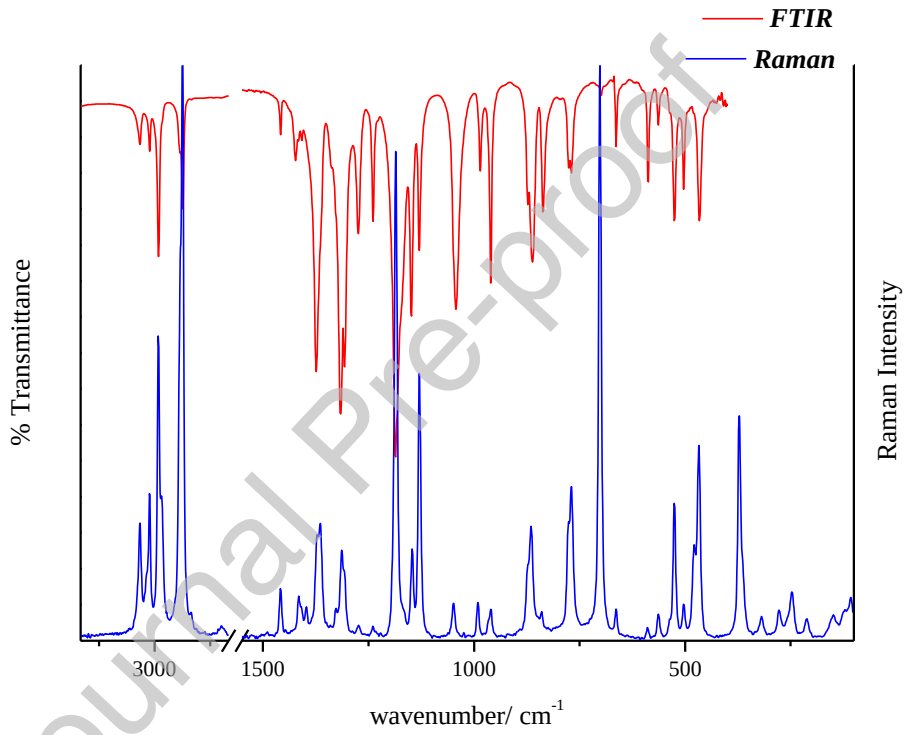

Figure 3. Infrared and Raman spectra of solid **TFMSMS.**

The C-H stretching modes are located at around 3000 cm^{-1} (**Table S2, Figure S1**).

The bands located at 3022 cm^{-1} and 2989 cm^{-1} in the Raman and IR spectra, respectively, are assigned to the CH_3 antisymmetric stretching modes, while the symmetric one appears at 2924 cm^{-1} and 2929 cm^{-1}, respectively (**Table S2**). The bands at 3040 cm^{-1} and 3013 $cm^{-1}$are attributed to the CH_2 groups' antisymmetric stretching and the absorptions at 2980 cm^{-1} and 2931 cm^{-1} to the symmetric ones. This assignment

corresponds to the *C10* conformer, (**Figure S1**) and no bands corresponding to the *C2* and *C5* conformers are observed.

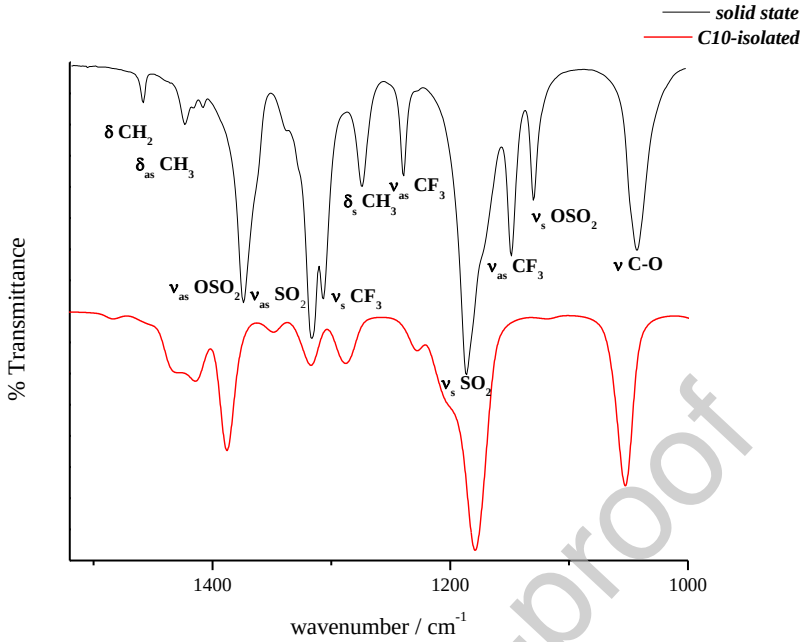

Figure 4. Experimental and calculated (B3LYP/6-311++G(3df) IR spectra of **TFMSMS** in the 1500-1000 cm^{-1} region.

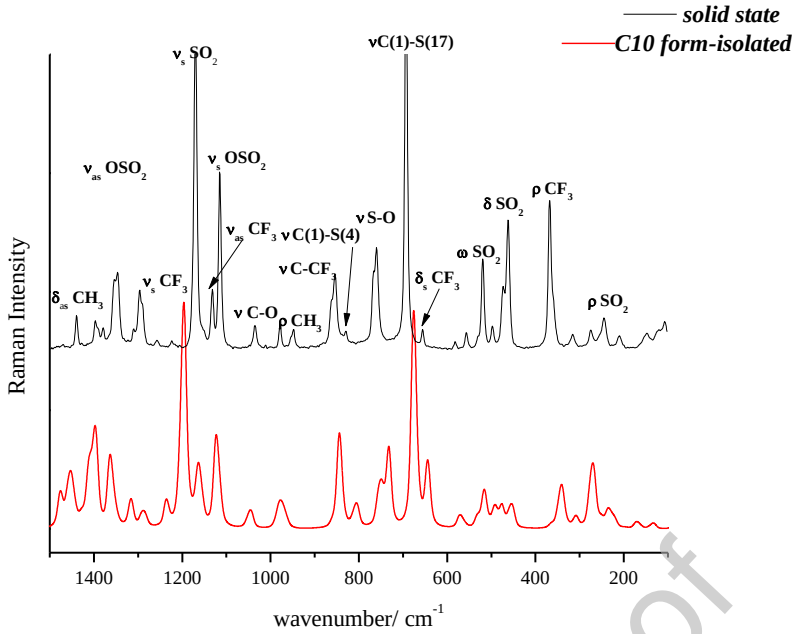

Figure 5. Experimental and calculated (B3LYP/6-311++G(3df)) Raman spectra of **TFMSMS** in the 1500-100 cm^{-1} region.

The CF_3 and SO_2 characteristic stretching bands appear in the region of 1500-1300 cm^{-1} (**Figures 4-5**). The IR absorptions at 1173 and 1148 cm^{-1} are assigned to the antisymmetric stretchings of the CF_3 group, and the symmetric one appears at 1274 cm^{-1}. In this case, the experimental and calculated assignments agree ($\nu_{as}CF_3 < \nu_sCF_3$) and the frequency difference between both modes is consistent with those observed for $CF_3SO_2OCH_2CF_3$ and $CCl_3SO_2OCH_2CF_3$ [44,45] and with the theoretical predictions.

The SO_2 antisymmetric and symmetric stretching modes are located in the 1357-1467 cm^{-1} and 1140-1157 cm^{-1} regions, respectively, for the CF_3SO_2X (X = F, OH, NH_2, CH_3, OCH_2CF_3) molecules. [10,41-45]

Figure 4 shows the experimental and calculated infrared spectra of the TFMSMS in the stretching region of the SO_2 group. There are clearly observed four bands corresponding to both SO_2 groups present in the molecule, sulfonate ($S(18)O_2$) and sulfone ($S(17)O_2$). Two intense bands at 1372 and 1130 cm^{-1} are assigned to the ν O-$S(18)O_2$ asymmetric and symmetric modes, respectively. The two very strong bands at 1316 cm^{-1} and 1185 cm^{-1} are assigned to the ν $S(17)O_2$ asymmetric and symmetric modes, respectively. In

the Raman spectrum, the symmetric stretch modes of the OSO_2 and SO_2 modes appear as strong bands at 1186 and 1130 cm^{-1}, respectively. (**Figure 5)**

The remaining bands corresponding to the vibrations of the $S(18)O_2$ group appear at relatively low frequencies: 525 cm^{-1} (wagging, IR); 503 cm^{-1} (bending, IR), 366 cm^{-1} (rocking, Raman) and 315 cm^{-1} (twisting, Raman). Besides, the infrared bands at 525 cm^{-1} (wagging, IR), 466 cm^{-1} (bending, IR) and the Raman bands at 245 cm^{-1} (twisting) are assigned to the $S(17)O_2$ group, which are also supported by computed and previous results. [10,41-45] (**Table S2-Figs 5, 6)**

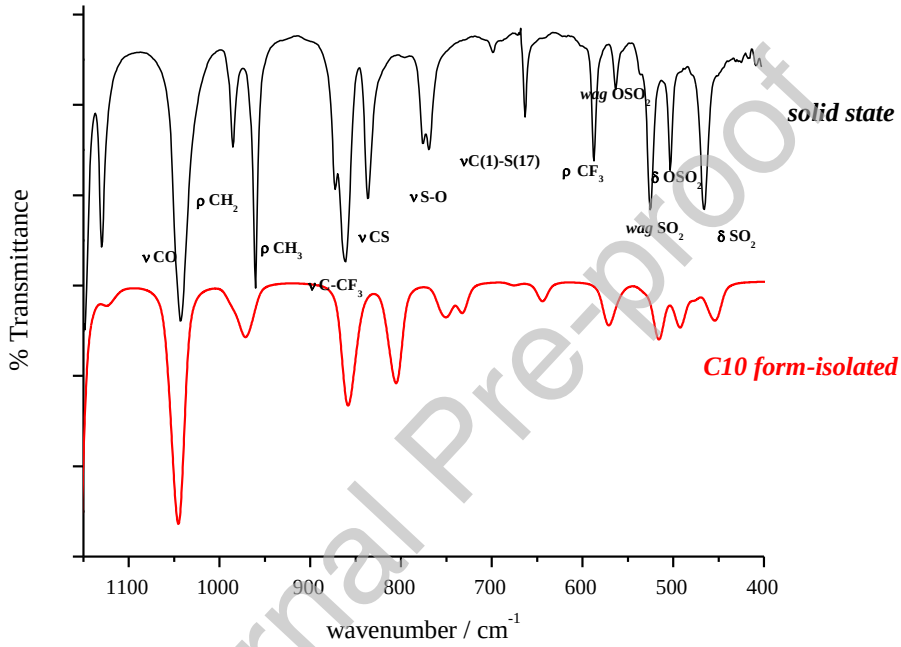

Figure 6. Experimental and calculated FTIR spectra of **TFMSMS** in the 1000-400 cm^{-1} region.

The IR bands at 1054, 836 and 775 cm^{-1} (**Figure 6)** are attributed to the C-O, C-CF_3, and S-O stretchings, respectively. The descriptions were based on the analysis of the atomic displacement analysis and by comparison with Clomesone. [10] The location of C-S stretching mode depends on the environment and the band at 769 cm^{-1} corresponds to ν C-SO_2 and ν S-CH_2, while the band at 669 $cm^{-1}$to ν S-CH_3 stretching.

3.3. NBO analysis

Natural bond orbital (NBO) analysis has often been used for evaluating the anomeric effect and to explain the origin of the internal rotation barrier. The NBO analysis allows to estimation of the energy of the molecule with the same geometry but in the absence of electronic delocalization. Moreover, only the steric and electrostatic interactions are taken into account through E_{Lewis}:

$\Delta E_{Total} = \Delta E_{Lewis} + \Delta E_{deloc.}$

ΔE_{Lewis} represents the energy of hypothetical localized species, described by an almost doubly occupied NBO determinant comprising the central electrons, lone pairs, and localized bonds of the Lewis structure. The delocalization energy change, ΔE_{deloc}, represents the hyper conjugative stabilization contribution to the rotational barrier that arises from bond → anti bond charge transfer.

Table 2. Calculated (B3LYP/6-311G(3df)]) contributions ($E_{Lewis,}$ $E_{deloc)}$ to the total energy of $CH_3SO_2CH_2SO_2OCH_2CF_3$ (**TFMSMS**) and $CH_3SO_2CH_2SO_2OCH_2CH_2Cl$ (Clomesone).

Compound	E_{total}[a]	ΔE_{total}[b]	E_{Lewis}[a]	ΔE_{Lewis}[b]	E_{deloc}[a]	ΔE_{deloc}[b]
TFMSMS	-1628.97769	0.00	-1625.72682	0.00	3.251	0.00
Clomesone	-1790.76732	-161.8	-1788.06322	-162.3	2.704	0.547

[a]Absolute energies in Hartrees

[b]Relative energies in kJ mol^{-1}

NBO calculations for TFMSMS and Clomesone were performed for monomers at the B3LYP/6-311(3df) level of theory. **Table 2** presents the contributions due to the localized (E_{Lewis}) and delocalized (E_{deloc}) electron density for the crystal structure. The results show that the delocalization energy plays a significant role in the **TFMSMS** stabilization, while for Clomesone are the electrostatic interactions.

The role of hyper conjugative interactions in the *gauche* conformer stabilization has been assessed using NBO analysis, where the hyperconjugation represents the transfer of an electron between a lone pair or bonding orbital and an antibonding orbital. The main interaction energies established between the orbitals were calculated for the B3LYP/6-311G(3df) level (**Table 3**). The most important interactions can be observed for the O12 atom lone pairs delocalization to the σ*S(17)-C(1), σ*S(18)-C(5) and σ*S(8)-C(5) antibonding orbitals; this sigma electrons donation influences the C(1)-S(17)-C(5)-S(18) and S(17)-C(5)-S(18)-O(12) dihedral angles, in which such atoms are

involved. Consequently, the *gauche* form is the preferred conformation of the different groups of the molecule.

A strong hyper conjugative interaction occurs from the O (13,14,15,16) atoms towards the anti-bonding orbitals σ*C(5)-S(17) and σ*C(5)-S(18) therefore, these antibonding orbitals have a higher population and a longer bond distance. (**Table S4**). This behavior can be proved experimentally, since the C(5)-S(18) and C(5)-S(17) stretching appear at a lower frequency than the corresponding to C(1)-S(17) bond. LP(π)O(15/16) → σ*S(18)-O(12) is also a relevant interaction with an average value of 130.0 kJ mol^{-1}, responsible for the large electronic delocalization in the sulfonate group. The greatest delocalization energy in **TFMSMS** is originated by LP(π)O(15/16) → σ*S(18)-O(12) charge transfer, increasing the stability of the SO_2-O group. Therefore, this sulfonate is a good donor of reactive groups with higher values than Clomesone, [10] in accordance with the experimental evidence that **TFMSMS** is a better "antibacterial agent.

The donated electron density through a mesomeric effect (+ M) by the three F atoms, can be observed in the LP(π)F →σ* C(8)-$C(11)_{average}$ delocalization, with a value of 29 kJ. In turn, the inductive effect exerted on the structure by the CF_3 group favors the increase of the electronic delocalization in the SO_2-O group with respect to Clomesone. It was found (REF) that, at pH values below the pKa of Clomesone, the main degradation products were chloroethanol and (methylsulfonyl) methanesulfonate, produced by the cleavage of a C-O bond instead of a S-O one. However, the CF_3 group converts the TFMSMS into a more reactive and better antibacterial compound. There are weak intermolecular hydrogen bonds between the O(13,14,15,16) atoms and the hydrogen atoms of the CH_2 and CH_3 groups, with energy values between 2-4 kJ mol^{-1}.

Tabla 3. Relevant hyperconjugative interactions (kJ mol^{-1}) for **TFMSMS**, calculated at the B3LYP/6-311G(3df) level.

Donor (*i*) → Acceptor (*j*)[a]	***ΔE*** **/** kJ/mol
LP(σ)O(12) →σ*S(18)-O(15)	14.13
LP(σ)O(12) →σ*S(18)-O(16)	6.48
LP(π)O(12) →σ*C(5)-S(17)	5.52
LP(π)O(12) →σ*C(5)-S(18)	21.40
LP(π)O(12) →σ* C(8)-C(11)	26.38
LP(π)O(12) →σ* C(8)-F(21)	4.43
LP(π)O(12) →σ* S(18)-O(15)	**2.59**

LP(π)O(12) →σ* S(18)-O(16)	**15.30**
LP(σ)O(15) →σ*C(5)-S(18)	4.64
LP(σ)O(15) →σ*S(18)-O(16)	7.27
LP(π)O(15) →σ* C(8)-H(10)	2.42
LP(π)O(15) →σ* C(5)-S(18)	**87.95**
LP(π)O(15) →σ* S(18)-O(16)	**90.96**
LP(π)O(15) →σ* S(18)-O(12)	**139.24**
LP(σ)O(16) →σ*C(5)-S(18)	3.68
LP(σ)O(16) →σ*S(18)-O(15)	6.86
LP(π)O(16) →σ* C(5)-H(7)	3.97
LP(π)O(16) →σ* C(5)-S(18)	**81.76**
LP(π)O(16) →σ* S(18)-O(15)	**91.42**
LP(π)O(16) →σ* S(18)-O(12)	**128.66**
LP(σ)O(13) →σ*C(1)-S(17)	3.85
LP(σ)O(13) →σ*C(5)-S(17)	2.72
LP(σ)O(13) →σ*S(17)-O(14)	5.85
LP(π)O(13) →σ* C(1)-H(3)	3.51
LP(π)O(13) →σ* C(1)-S(17)	81.64
LP(π)O(13) →σ* C(5)-S(17)	104.04
LP(π)O(13) →σ* S(17)-O(14)	95.10
LP(σ)O(14) →σ*C(1)-S(17)	3.51
LP(σ)O(14) →σ*C(5)-S(17)	2.67
LP(σ)O(14) →σ*S(17)-O(13)	5.43
LP(π)O(14) →σ* C(1)-H(2)	3.80
LP(π)O(14) →σ* C(1)-S(17)	80.05
LP(π)O(14) →σ* C(5)-S(17)	92.04
LP(π)O(14) →σ* C(5)-S(18)	9.66
LP(π)O(14) →σ* S(17)-O(14)	93.05
LP(π)F →σ* C(8)-C(11)$_{average}$	29.26

[a]LP denotes electron lone pair, (for atom numbering see **Figure 2**).

3.4. AIM Analysis

Bader's Atoms in Molecules (AIM) quantum theory performs a topological analysis of electronic charge density and its Laplacian, at the bond critical point (BCP), allowing to know the nature of the interactions. The results predict intramolecular hydrogen bonds, which give rise to the formation of six-members rings.

Table 4 shows the properties of the electronic charge density in some selected BCP´s for **TFMSMS**. The ρ(r) and $\nabla^2\rho(r)$ values for the CC, CS, SO, CF and S=O bonds are typical of shared or covalent interactions, which are dominated by a contraction of ρ(r) towards the bond, leading to its accumulation in the internuclear region.

The values of ρ(r) are within the range of 0.177 - 0.323 au and $\nabla^2\rho(r)$ are in the interval of -0.130 to -0.860) au. The high electron density value for the C-C bond and a positive value of |λ1|/λ3 is striking, indicating a C-C bond with equally distributed charges and is highly covalent.

Table 4 shows the topological and energetic properties for two localized intramolecular hydrogen bonds. The positive values of ρ(r) and $\nabla^2\rho(r)$ are in the range of 0.00625/0.01199) and 0.2238/0.04900, respectively, typical for weak hydrogen bonds. Charge density and Laplacian are within the interval proposed by Koch and Popelier [46] for H bond interactions: 0.002–0.034 au and 0.024–0.139 au, respectively. Intramolecular bonds are very weak and it is in accordance with the results obtained by NBO.

Table 4. Local topological properties of the electron charge density at the bond, ring, and cage critical points in the intermolecular region, in the TFMSMS studied**.**

Bond	**ρ(r)**	**$\nabla^2(\rho)$**	$\lvert\lambda_1\rvert/\lambda_3$
C(1)-S(17)	0.209	-0.424	1.250
C(5)-S(17)	0.197	-0.380	1.192
S(18)-C(5)	0.205	-0.402	1.227
C(8)-C(11)	0.270	-0.700	1.365
O(12)-S(18)	0.234	-0.054	0.562
C(8)-O(12)	0.238	-0.404	0.956
S(18)=O(15)	0.326	-0.888	0.291
S(18)=O(16)	0.319	-0.816	0.300
O(16)···H-C(1)	0.011	-0.036	0.180
S(17)=O(13)	0.305	-0.732	0.311
S(17)=O(14)	0.313	-0.766	0.307
O(14)···H-C(8)	0.008	0.036	0.095
C(11)-F $_{average}$	0.290	-0.498	0.784

In **Figure 7** (a), the large circles correspond to attractors or (3, −3) nuclear critical points (NBP, attributed to the positions of the atomic nuclei), lines connecting the nuclei are the PA and the small circles are the critical points, BCP (3, −1), obtained from the topological analysis of the electron density. The presence of a BCP and its associated virial pathway provides a universal indicator of bonding between atoms.

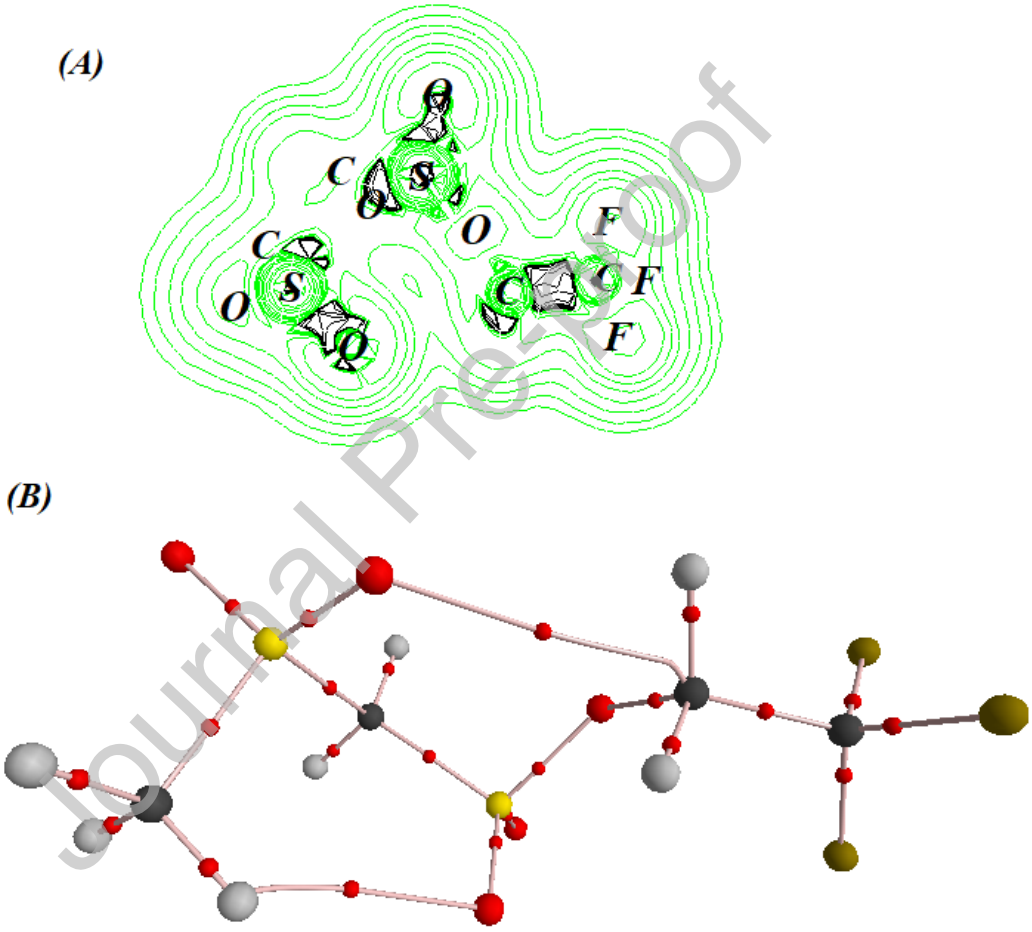

Figure 7. (a). Laplacian contour map, showing the same orientation of the molecule, atoms in the equivalent plane are indicated by circles. **(b)** Topological graphs to show bond and ring pathways (solid lines joining adjacent atoms and those involved in hydrogen bonding interactions), and bond and ring critical points.

3.5. Bacterial growth and Biofilm inhibition

***Pseudomonas aeruginosa* PAO1**

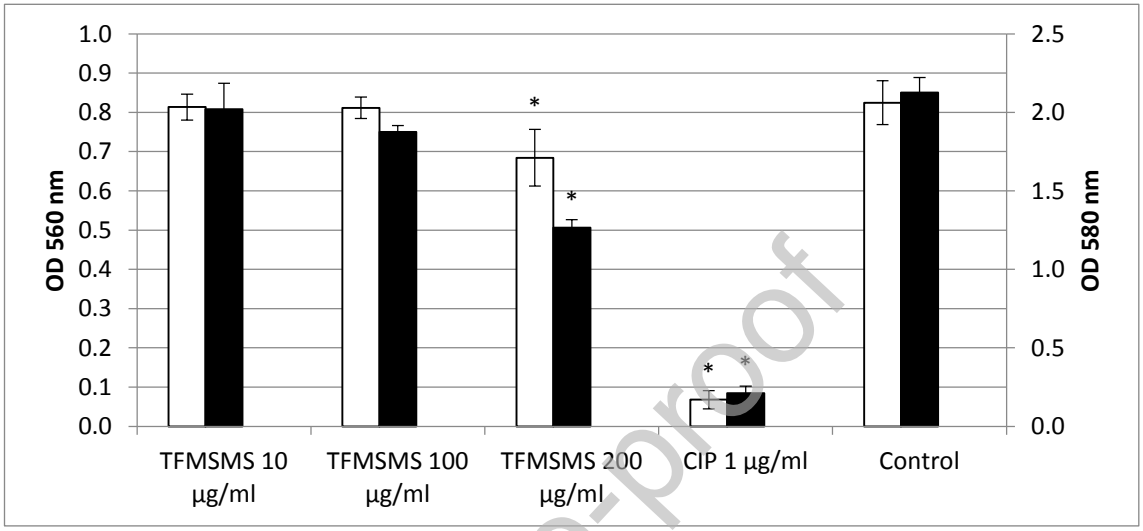

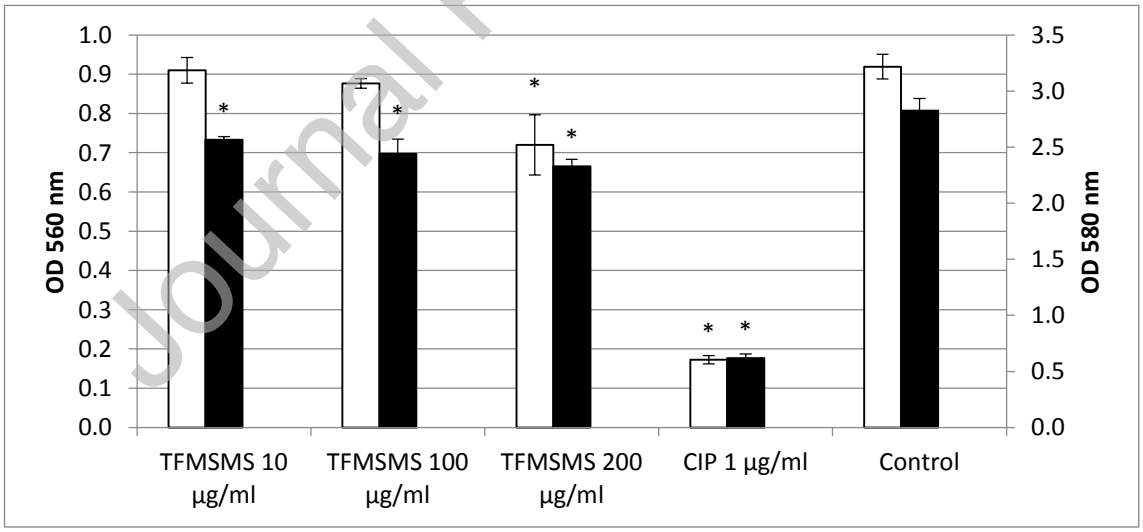

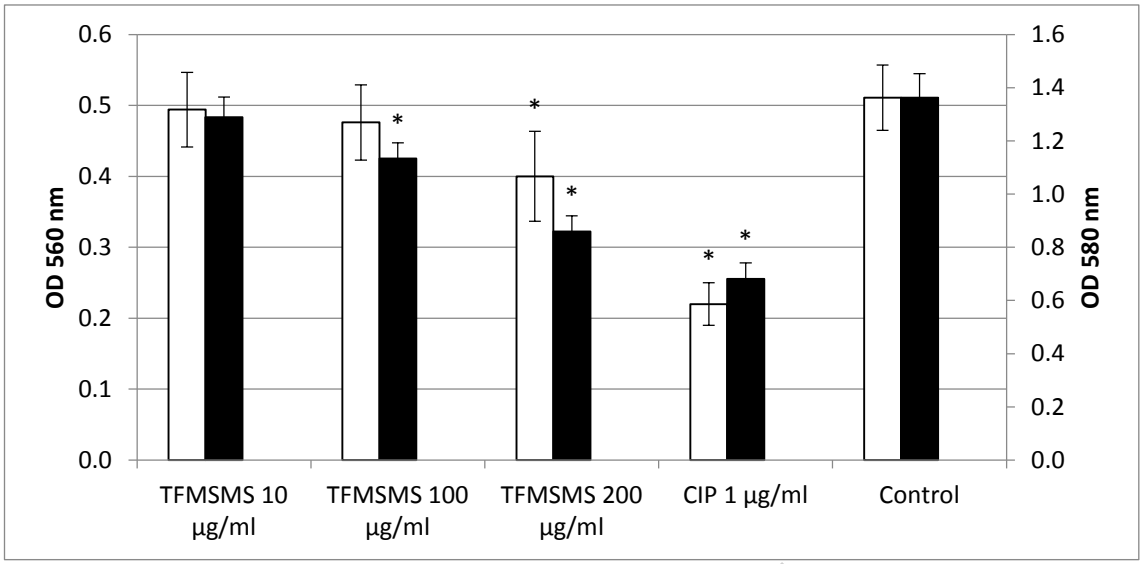

Figure 8. Growth (□) and biofilm formation (■) by *P. aeruginosa* PAO1 cultures grown in LB broth in absence and presence of 10, 100 and 200 µg/ml of **TFMSMS**. CIP (Ciprofloxacin) 1 µg/ml was used as inhibitor control. Results are expressed as means ± standard deviation (n=5). *Represents statistically significant differences (p-value ≤ 0.05) compared with the untreated control (DMSO 2,5%).

***Pseudomonas aeruginosa* PA14**

Figure 9. Growth (□) and biofilm formation (■) by *P. aeruginosa* PA14 cultures grown in LB broth in absence and presence of 10, 100 and 200 µg/ml of **TFMSMS**. CIP (Ciprofloxacin) 1 µg/ml was used as inhibitor control. Results are expressed as means ± standard deviation (n=5). *Represents statistically significant differences (p-value ≤ 0.05) compared with the untreated control (DMSO 2,5%).

***Staphylococcus aureus* ATCC 6538**

Figure 10. Growth (□) and biofilm formation (■) by *S. aureus* ATCC 6538 cultures grown in LB broth in absence and presence of 10, 100, and 200 µg/ml of **TFMSMS**. CIP (Ciprofloxacin) 1 µg/ml was used as inhibitor control. Results are expressed as means ± standard deviation (n=5). *Represents statistically significant differences (p-value ≤ 0.05) compared with the untreated control (DMSO 2,5%).

According to Figures (**8**, **9,** and **10**), TFMSMS can inhibit the growth of the three bacteria understudy at the higher concentration assayed (200 µg/ml) in a statistically significant value. The growth inhibition was 16, 20, and 22% for the strains *P .aeruginosa* PAO1, *P. aeruginosa* PA14, and *Staphylococcus aureus* ATCC 6538, respectively.

There is a linear correlation between growth inhibition and biofilm formation for *P. aeruginosa* strain PA14

However, the biofilm formation showed a significant inhibition since 100 ug/ml for the other strains. At 200 ug/ml, the biofilm inhibition was 38 and 35% by *P. aeruginosa* PAO1 and *S. aureus* ATCC 6538. Therefore, it suggested that the TFMSMS affects biofilm formation by another mechanism than bacterial growth inhibition.

Previous studies indicated that a compound is considered active when it is active until 100-200 ug/ml (Rios and Reccio, 2005). For this reason, TFMSMS is poor active against bacterial development. However, it could be considered active against bacterial biofilm formation.

According to the obtained results, there is no direct correlation between biofilm inhibition and bacterial growth; we studied the effect of t TFMSMA on cell-cell communication that induces biofilm formation.

The inhibition on the autoinducer effect was studied using the biosensor *Chromobacterium violaceum* CV26 (**Figure 11**)

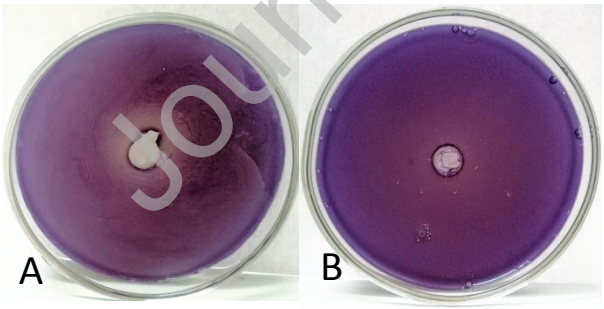

Figure 11. Effect on violacein production of C*hromobacterium violaceum* CV026 by: A) **TFMSMS** (200 ug/mL); B) Control (DMSO 2%). The turbid halo of inhibition is 8.7 ± 0.6 mm

Inhibition of QS was detected by a zone of colorless but viable cells around the sample. At 200 ug/mL, TFMSMS inhibits QS system-associated pigment production: This result explains the higher biofilm inhibition concerning growth inhibition.

A complex of methansulfonate is used for the administration of Colistin. Colistin methanesulfonate (CMS) is a hydrolyzed prodrug after intravenous administration to produce several derivatives, predominately Colistin's active drug. This complex is used to control the colonization of the respiratory tract by *P. aeruginosa*, preventing the development of pneumonia since its toxicity is significantly reduced compared to Colistin. [41]

This complex of methansulfonate was the only previously studied concerning biofilm inhibition. The bactericidal effect of colistin methanesulfonate on biofilm-forming cells of multidrug-resistant *P. aeruginosa* strain was poor compared with those on the planktonic cells. These *in vitro* obtained results indicated that the efficacy of administered colistin methanesulfonate depends on the formed biofilm resistance. [47] The present is the first study of a methansulfonate complex on biofilm formation, different from the CMS, which also shows QS inhibition.

CONCLUSIONS

Trifluoroethyl metansulphonate (methylsulfonyl), **TFMSMS**, was prepared as reported in the literature with modifications. The obtained white crystalline solid was suitable for spectroscopic and structural studies but not for X-ray diffraction. The concept of "transferability" of conformational behavior, that is, the properties by which similar groups adopt the same conformation when they are present in different molecules was assumed for the structure elucidation. The calculated bond distances for **TFMSMS** and Clomesone are very similar, except for the O(12)-C(8) distance, which results shorter for **TFMSMS**. This can be explained by the greater inductive effect caused by the replacement of CH_2Cl by CF_3 group. The donated electrons density through a mesomeric effect (+ M) by the presence of the three F atoms was evidenced in the $LP(\pi)F \rightarrow \sigma^* C(8)\text{-}C(11)_{average}$ delocalization, with a value of 29 kJ. In turn, the inductive effect exerted by the CF_3 group on the structure, favors the increase of the electronic delocalization in the SO_2-O group compared to Clomesone. The **TFMSMS** vibrational data (IR and Raman) were used as a basis to perform an approximate description of the vibrational modes.

TFMSMS inhibits the growth and biofilm formation of the pathogenic bacteria P. aeruginosa PA14, P. aeruginosa PAO1, and S. aureus ATCC 6538. On the other hand,

TFMSMS can inhibit the *Quorum sensing* system in Gram-negative bacteria. Its effect on the biofilm could be due to the decrease in development and the inhibition of its bacterial communication system. In the future, these results will also support the study of interactions between **TFMSMS** molecules with model lipid membrane systems. In this way, a general understanding could be reached to elucidate the action mechanisms at a molecular level in more complex biological systems.

Credit Author Statement

The authors declare that they have no known competing financial interests or personal relationships that could have appeared to influence the work reported in this paper.

Declaration of interests

The authors declare that they have no known competing financial interests or personal relationships that could have appeared to influence the work reported in this paper.

Acknowledgments

The authors wish to thank Consejo de Investigaciones de la Universidad Nacional de Tucumán (CIUNT), Consejo Nacional de Investigaciones Científicas y Técnicas, PIP 002 and PIP 0359 (CONICET), ANPCyT (PICT2013- 0697, PICT2019-02578), PICT 2018-02071), Universidad Nacional de La Plata (UNLP) and Departamento de Ciencias Básicas de la Universidad Nacional de Luján (UNLu) for financial support.

References

[1] D. J. Dykes, W. R. Waud, S. D. Harrison, Jr., W. R. Laster, Jr., D. P. Griswold, Jr., Y. F. Shealy and J. A. Montgomery, *Cancer Research*, 49 (1989) 1182-1186.

[2] Tong, K. W. Kohn and D. B. Ludlum, *Cancer Res*., 42 (1982) 4460-4464.

[3] C. T. Combar, W. P. Tong and D. B. Ludlum, *Biochem.Pharmacol*, 29 (1980) 2639-2643.

[4] G. P. Wheeler, B. J. Bowden and R. F. Struck, *Cancer Res*., 35 (1975) 2974-2984.

[5] N. W. Gibson, J. A. Hartley, J. M. Strong and K. W. Kohn, *Cancer Res*., 46 (1986) 553-557.

[6] T. Siod, W.P. Ozimin, M. Ho, H. Koroniak, T.M. Krygowski, Toward a Physical Interpretation of Substituent Effects: The Case of Fluorine and Trifl uoromethyl Groups, *J. Org. Chem.* 79, 16 (2014) 7321–7331.

[7] B.K. Park, N.R. Kitteringham, Effects of fluorine substitution on drug metabolism: Pharmacological and toxicological implications, Drug Metab. Rev. 26 (1994) 605–643.

[8] B.E. Smart, Fluorine substituent effects (on bioactivity), J. Fluor. Chem. 109 (2001) 3–11.

[9] Yale, The Trifluoromethyl Group in Medicinal Chemistry, J. Med. Chem. 1 (1959) 121–133.

[10] E. Galvan, M. E. Defonsi Lestard, O. E. Piro, G. Echeverria, R. D. I. Molina, M. E. Arena, S. E. Ulic, M. E. Tuttolomondo and A. Ben Altabef, *New J. Chem.*, 42(2018)11073-11084.

[11] A.E. Reed, R.B. Weinstock, and F. Weinhold, J. Chem. Phys., 83 (1985) 735-746.

[12] R.F.W. Bader, Atoms in and Molecules. A Quantum Theory, Clarendon Press, Oxford. (1990)

[13] M.E. Arena, A.N. Ramos, J.C. Valdez, *Academic Publishing GmbH& Co. Saabrücken, (*2012) - ISBN. 978-3-8484-5021-3.

[14] E. Cartagena, K. Marcinkevicius, C. Luciardi, G. Rodríguez, A. Bardón, M.E. Arena,*Journal of Pest Science*, 87 (2014) 521–530.

[15] R. E. D'Almeida, R.D.I. Molina, C.M. Viola, M.C. Luciardi , C. Nieto Peñalver, A. Bardón, *Bioorganic Chem.*, 73 (2017) 37-42.

[16] A. Di Santo, D.M. Gil, F. Pomiro, O.E. Piro, G.A. Echeverria, M. Arena, C. Luciardi, R.E. Carbonio, A. Ben Altabef, *Inorg.Chimica Acta*, 436 (2015) 16-22.

[17] M.C. Luciardi, M.A. Blázquez, E. Cartagena, A. Bardón, M.E. Arena, *Science and Technology*, 68 (2016) 373-380.

[18] Y. Fulmer Shealy, C. A. Krauth, R. F. Struck, J. A. Montgomery, *J. Med. Chem.*, 26 (1983) 1168-1173

[19] Gaussian 03, Revision C.01, M.J. Frisch, G.W. Trucks, H.B. Schlegel, G.E. Scuseria, M.A. Robb, J.R. Cheeseman, J.A. Montgomery, Jr., T. Vreven, K.N. Kudin, J.C. Burant, J.M. Millam, S. S.Iyengar, J. Tomasi, V. Barone, B. Mennucci, M. Cossi, G. Scalmani, N. Rega, G.A. Petersson, H. Nakatsuji, M. Hada, M. Ehara, K. Toyota, R. Fukuda, J. Hasegawa, M. Ishida, T. Nakajima, Y. Honda, O. Kitao, H. Nakai, M. Klene, X. Li, J.E. Knox, H. P.Hratchian, J.B. Cross, V. Bakken, C. Adamo, J. Jaramillo, R. Gomperts, R.E. Stratmann, O. Yazyev, A.J. Austin, R. Cammi, C. Pomelli, J.W. Ochterski, P.Y. Ayala, K. Morokuma, G.A. Voth, P. Salvador, J.J. Dannenberg, V.G. Zakrzewski, S. Dapprich, A.D. Daniels, M.C. Strain, O. Farkas, D.K. Malick, A. D.Rabuck, K. Raghavachari, J.B. Foresman, J.V. Ortiz, Q. Cui, A.G. Baboul, S.

Clifford, J. Cioslowski, B.B. Stefanov, G. Liu, A. Liashenko, P. Piskorz, I. Komaromi, R.L. Martin, D.J. Fox, T. Keith, M. A. Al-Laham, C.Y. Peng, A. Nanayakkara, M. Challacombe, P.M.W. Gill, B. Johnson, W. Chen, M.W. Wong, C. Gonzalez, J.A. Pople, *Gaussian, Inc., Wallingford* CT. (2004)

[20] M.J. Frisch, et al. Gaussian 09, Revision B.01, Gaussian, Inc.: Wallingford, CT, USA (2009)

[21] W. J. Hehre, R. Ditchfield, J. A. Pople, J. Chem. Phys.,56 (1972) 2257-2261.

[22] P. C. Hariharan, J. A. Pople, Theor. Chim.Acta, 8 (1973) 213-222.

[23] M. S. Gordon, Chem. Phys. Lett., 76 (1980) 163-168.

[24] A. D. McLean, G. S. Chandler, J. Chem. Phys., 72 (1980) 5639-5648.

[25] R. Krishnan, J. S. Binkley, R. Seeger, J. A. Pople, J. Chem. Phys., 72 (1980) 650-654.

[26] A. D. Becke, Phys. Rev. A 38 (1988) 3098

[27] A. D. Becke, J. Chem. Phys. 98 5648 (1993).

[28] C. Lee, W. Yang, R. G. Parr, *Phys. Rev. B*, , 37 (1988) 785-789.

[29] J. P. Perdew, *Phys. Rev. B, 33* (1986) 8822-24.

[30] E.D. Glendening, J. K. Badenhoop, A. E. Reed, J. E. Carpenter and F. F. Weinhold, NBO 3.1 Theoretical Chemistry Institute, University of Wisconsin, Madison, WI, (1996).

[31] J.P. Foster and F. Weinhold, J. Am. Chem. Soc., 102 (1980) 7211-7218.

[32] F. Biegler-König and J. Schönbohm, AIM 2000 version 2.0, University of Applied Science, Bielefeld, Germany, (2002).

[33] B. Nielsen, A. J. Holder, GaussView, User's Reference; GAUSSIAN Inc.: Pittsburgh, PA, (1997–1998).

[34] H. Yoshida, K. Takeda, J. Okamura, A. Ehara and H. Matsuura, J. Phys. Chem. A, 106 (2002) 3580.

[35] M. H. Jamroz, VEDA Industrial Chemistry Research Institute, 8 Rydygiera Street, 01-793 Warsaw, Poland.

[36] G. O'Toole and R. Kolter, *Molecular Microbiology*, 28 (1998) 449-451.

[37] K. H. McClean, M. K. Winson, L. Fish, A. Taylor, S.R. Chhabra, M. Camara, M. Daykin, J. H. Lamb, S. Swift, B.W. Bycroft, *Microbiology*, 143 (1997) 3703–3711.

[38] S. Manner, D. M. Goeres, M. Skogman, P. Vuorela and A. Fallarero. Sci. Rep., 7 (2017) 1211-1222.

[39] K. Marumo, D. Komukai, M. Hirose, H. Nakamura, H. Tanaka, K. Ugajin, G. Nagashima, Yoshimura, *J. Infect Chemother.,* 19 (2013) 348–351.

[40] R.L. Nation, J. Li, *Hodder Arnold*, (2010) 955-970.

[41] J.E. Galván , O., G. Echeverria , R.D.I. Molina , M.E. Arena , E. Contreras Aguilar , S.E. Ulic , M.E. Tuttolomondo , A. Ben Altabef, J. Mol. Struc.,1230 (2021), 129655.

[42] J. E. Galván, E. Contreras Aguilar, M. E. Defonsi Lestard, M. E. Tuttolomondo, S. E. Ulic, A. Ben Altabef. Inorganica Chimica Acta, 455 (2017) 254-261.

[43] M.E. Defonsi Lestard, L.A. Ramos Guerrero, M.E. Tuttolomondo, S.E. Ulic and A. Ben Altabef. Vib. Spectrosc.,59 (2012) 40-46.

[44] M. E. Tuttolomondo, L. E. Fernández, A. Navarro, E .L. Varetti, A. Ben Altabef. Spectrochim. Acta, 60A (2004) 611.

[45] M. E. Tuttolomondo, A. Navarro, E. L. Varetti, A. Ben Altabef. Spectrochim. Acta, 61A(2005)1011-1019.

[46] U. Koch, P. L. A. Popelier, *J. Phys. Chem.*, 99(24) (1995) 9747-9754.

[47] K. Marumo, D. Komukai, M. Hirose, H. Nakamura, H. Tanaka, K. Ugajin, G. Nagashima, Yoshimura, *J. Infect Chemother.,* 19 (2013) 348–351.